Technical Paper

ISSN 1997-1400 Int. J. Pavement Res. Technol. 2(3):115-122

Modeling HMA Bulk Specific Gravities: A Theoretical and Experimental Investigation

Filippo G. Pratico'[1+], Antonino Moro[2], and Rachele Ammendola[2]

Abstract: Bulk specific gravity, G_{mb}, is of outstanding importance in bituminous mixes. Life cycle costs, contract requirements, and Quality Control/Quality Assurance procedures are strongly dependent on the effective G_{mb} obtained by suitable design and construction, and compliance with a number of boundary conditions. There are many ways to estimate G_{mb}, and within-method variance is appreciable. The "transportability" of a G_{mb} determined according to a given standard to another standard is therefore a critical issue. Our objective was to study relationships between G_{mb} values determined using a given standard to G_{mb} estimates calculated by applying other standards. We derived a model, and conducted experiments using five different methods. The model evaluates the elementary volumes that contribute to differences among the five considered methods. A tendency toward a common maximum value is assumed. The results are analyzed and interpreted, and the conceptual framework validated. Useful relationships between specific gravities determined by different methods are derived and analyzed. Power-asymptotic curve analysis yielded an algorithm well-grounded in logic to solve the issue of G_{mb} transportability.

Key words: *Bulk specific gravity; Hot mix asphalts; Osculatory volume.*

Problem Statement

Bulk specific gravity, G_{mb}, measures the specific gravity of a compacted Hot Mix Asphalt (HMA) sample. G_{mb} is of outstanding importance in evaluation of bituminous mixes. Life cycle costs, contract requirements, and Quality Control/Quality Assurance procedures are strongly affected by the effective G_{mb} values obtained by suitable design and construction, and application of appropriate boundary conditions.

Although specific gravity is important, there are many different ways to determine G_{mb}, and many authors have attempted to find correlations among results obtained using the various procedures [1-8]. In this study, we construct a model to evaluate differences between procedures and seek information on the transportability of G_{mb} values between such procedures.

The model is based on a conceptual framework in which variations between G_{mb} values of a given sample originate from a difference in the osculatory external volume (V_0) of the sample and the mix bulk volume (V_{mb}), termed the "roughness volume" R (Fig. 1). In the model, R corresponds to "extended" roughness (related to voids), V_{mb} is the mix bulk volume, V_0 is an osculatory (external) volume, using the terms of the Dimensional Method, R_{BS} is Bottom Surface Roughness, R_{LS} refers to Lateral Surface Roughness, whereas R_{US} corresponds to Upper Surface Roughness (Fig. 1).

Thus,

$$V_{mb} = V_0 - R \tag{1}$$

where

$$R = R_{BS} + R_{LS} + R_{US} \tag{2}$$

Each of these three components (volumes), the R_i values, can be split into three sub-components: Positive (P), Negative (N), and HyperNegative (HN):

$$V_{mb} = V_0 - R_{BS} - R_{LS} - R_{US} = V_0 - \left[R_{BSP} + R_{BSN} + R_{BSHN}\right] - \left[R_{USP} + R_{USN} + R_{USHN}\right] - \left[R_{LSP} + R_{LSN} + R_{LSHN}\right] \tag{3}$$

Theoretically, the differences among measurement methods can be explained by the following equation:

$$V_{mb} = V_0 - \left[R_{BSP} + R_{USP} + R_{LSP}\right] - \left[R_{BSN} + R_{USN} + R_{LSN}\right] - \left[R_{BSHN} + R_{USHN} + R_{LSHN}\right] \tag{4}$$

It results in: $$G_{mb} = \frac{P_{mb}}{V_{mb}\gamma_w} = F(V_0, R) \tag{5}$$

where G_{mb} is the bulk specific gravity, P_{mb} represents the (dry) mass of the bituminous mix, γ_w is the density of water at the same temperature, and F is a function. When R is small, the internal voids tend to be negligible, and, then:

$$\lim_{R\to 0} V_{mb} \cong V_0 \tag{6}$$

$$\lim_{R\to 0} G_{mb} \cong G_{mm} \tag{7}$$

where G_{mm} is the maximum theoretical specific gravity:

$$G_{mm} = \frac{P_b + P_a}{\left[V_b + V_a\right]\gamma_w} \tag{8}$$

In this equation P_b and V_b are the mass and volume of asphalt binder, respectively, whereas P_a and V_a refer to aggregates. Thus,

[1] Associate Professor, DIMET Department, Mediterranea University, Reggio Calabria, Italy.
[2] Research Assistant, DIMET Department, Mediterranea University, Reggio Calabria, Italy.
[+] Corresponding Author: E-mail filippo.pratico@unirc.it
Note: Submitted December 24, 2008; Revised February 18, 2009; Accepted February 20, 2009.

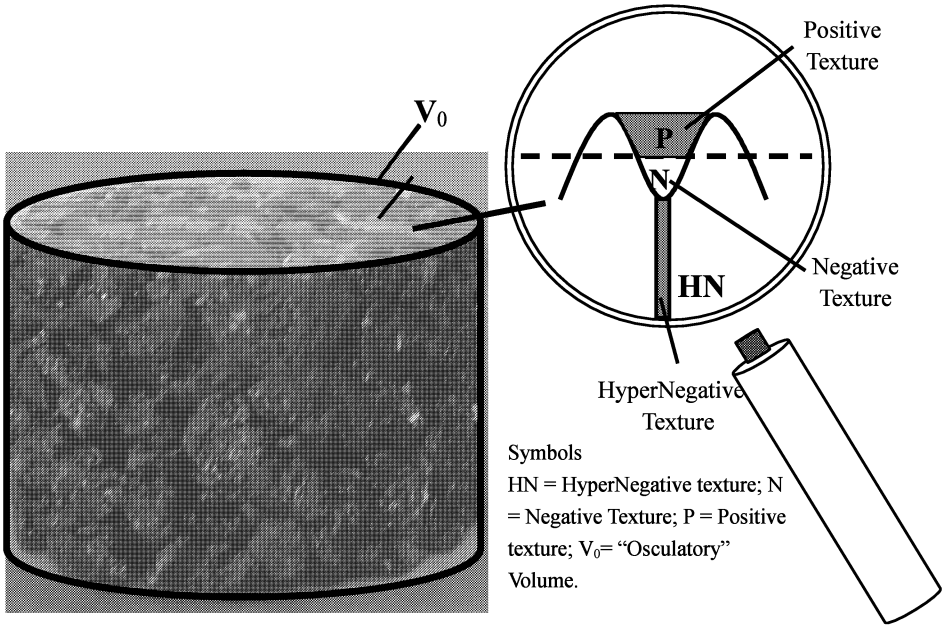

Fig. 1. Osculatory Volume of a HMA Specimen.

Eqs. (6) and (7) suggest pursuit of the G_{mb} transportability objective by consideration of the tendency toward restriction of the variability zone as G_{mb} increases. The approach of Eqs. (4-8) can be integrated with an analysis focused on solid *versus* fluid volumes (Fig. 2 shows the relevant schematic for the case saturated surface dry (SSD) *versus* paraffin-coated (FIN)):

$$V_{mbSSD} = \alpha_1 + \sum_{i=3}^{K} \alpha_i \tag{9}$$

$$V_{mbFIN} = \sum_{i=1}^{\xi} \alpha_i \tag{10}$$

where all α_i values are volumes and $\alpha_1 \equiv \alpha_S$ represents the solid volume (aggregate +bitumen), whereas each $\alpha_i, \forall i \neq 1$, corresponds to a fluid (such as air, water, or paraffin) volume. For mixes that are not too "open" , K may be assumed to be 4 and ξ to be 5; $\alpha_6 + \alpha_7$ represent paraffin.

In this case, and using Eqs. (9) and (10) above, the following equations are derived:

$$V_{mbSSD} = \alpha_1 + \alpha_3 + \alpha_4 \tag{11}$$

$$V_{mbFIN} = \alpha_1 + \alpha_2 + \alpha_3 + \alpha_4 + \alpha_5 \tag{12}$$

$$V_{mbFIN} = V_{mbSSD} + \alpha_2 + \alpha_5 \tag{13}$$

$$V_{mbFIN} > V_{mbSSD} \tag{14}$$

From Eqs. (5) and (14) it follows that:

$$G_{mbSSD} > G_{mbFIN} \tag{15}$$

Moreover, if $\alpha'_2 = \alpha_2 \gamma_w$ and $\alpha'_5 = \alpha_5 \gamma_w$, where γ_w represents the density of water, the following equations are obtained:

SSD: α_1: solid; α_2, α_5, α_6: air; α_3, α_4: water.

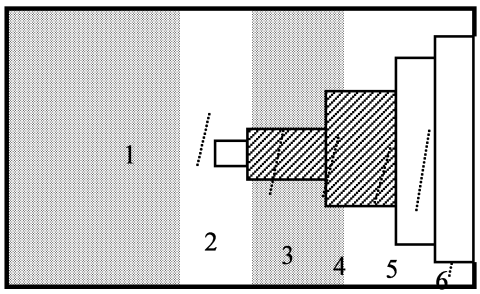

FIN: α_1: solid; α_2, α_3, α_4, α_5,: air; α_6, α_7: paraffin.

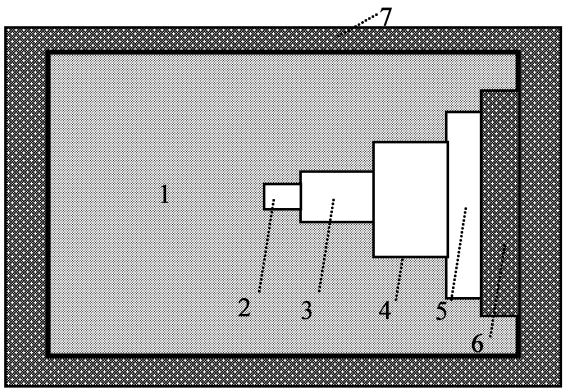

Fig. 2. Volumes α_i (Not in Scale).
Note. SSD: saturated surface dry; FIN: paraffin-coated.

$$\frac{1}{G_{mbFIN}} = \frac{1}{G_{mbSSD}} + \frac{\alpha'_2 + \alpha'_5}{P_{mb}} \tag{16}$$

$$\frac{100}{G_{mbFIN}} = \frac{100}{G_{mbSSD}} + \frac{\alpha'_2 + \alpha'_5}{P_{mb}} 100 \tag{17}$$

$$\Delta V_{SSD-FIN} = \frac{\alpha_2' + \alpha_5'}{P_{mb}} 100 = 100 \frac{G_{mbSSD} - G_{mbFIN}}{G_{mbFIN} G_{mbSSD}} \quad (18)$$

where $\Delta V_{SSD\text{-}FIN}$ is the percentage difference between the "specific" volumes of SSD and FIN. Similarly it is possible to define $\Delta V_{FIN\text{-}COR}$, $\Delta V_{COR\text{-}FILM}$, and $\Delta V_{FILM\text{-}DIM}$, where *COR*, *FILM*, and *DIM* are three different methods explained below.

Experimental Plan

The mixes tested are described below, and the procedures used are summarized in the following section.

Mixes

A total of 205 mixes were tested and five methods used for G_{mb} determination.

DGFCs (Dense-Graded Friction Courses) and PEMs (Porous European Mixes) were obtained (Fig. 3 and Table 1). For each set, a subset of specimens was used in composition analyses for asphalt binder content (CNR [Consiglio Nazionale delle Ricerche] n.38/73, EN [European Standard] 12697-1:2006), aggregate grading (CNR n.4/53, EN 12697-2:2008), and aggregate apparent specific gravity (CNR n. 63/78, EN 12697-5:2008) (Fig. 3 and Table 1). Fig. 3 shows aggregate gradations and Superpave requirements. NMAS is the Nominal Maximum Aggregate Size. Note that DGFCs generally conform to Superpave requirements (some Through Restricted Zone (TRZ), and some Below Restricted Zone (BRZ)). On the contrary, as is well known, PEM gradations are of the BRZ type and are outside control points.

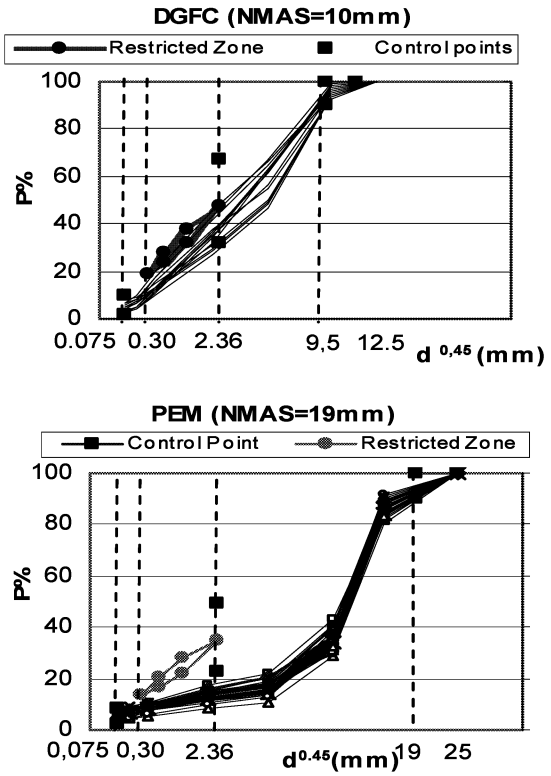

Fig. 3. Gradations.

Table 1. Composition of the Mixes Tested (Averages).

	% b	γ_g (g/cm^3)	NMAS (mm)	P_{200} (%)	S (%) (0,075/2)	Compaction
DGFC	5.5	2.726	10	4.4	31.1	in site
PEM	5.1	2.829	19	5.2	7.6	in site

Note: % b = asphalt binder content referred to aggregate weight; γ_g = aggregate apparent density; P_{200}(%)= filler content; S(%) = Sand content; NMAS = Nominal Maximum Aggregate Size

Procedures

Five different methods were considered:

- the dimensional method (DIM);
- four water displacement methods, being i) Saturated Surface Dry (SSD); ii) Paraffin (FIN); iii) Parafilm (FILM); and, iv), the Vacuum Sealing Method, VSD (COR).

In Table 2, algorithms and standards for each indicator are detailed.

The DIM is based on height and diameter/width measurements.

In water displacement methods, specimen volume is calculated by weighing in a water bath and outside of the water bath. In the SSD approach the specimen volume is calculated by subtracting the mass of the specimen in water from the mass of a SSD sample. The FIN method determines volume according to the water displacement principle but uses melted paraffin wax for the external sealing (we emphasize: not the filling) of a sample's internal air voids.

In the FILM method, a thin film is used to wrap the specimen and weights are obtained in and out of water. In the COR method,

Table 2. Main Procedures for G_{mb}

	Indicator	Algorithm	Standard
1.	G_{mbDIM} *(dimensional)*	$\frac{A}{V_{DIM}\gamma_w}$	AASHTO T 269 EN 12697-6:2003
2.	G_{mbFILM} *(parafilm)*	$\frac{A}{D'-E'-\frac{D'-A}{F}}$	ASTM D 1188 (abs>2%)
3.	G_{mbCOR} *(VSD)*	$\frac{A}{B'-E'-\frac{B'-A}{F_t}}$	ASTM D 6752
4.	G_{mbFIN} *(paraffin)*	$\frac{A}{D-E-\frac{D-A}{F_p}}$	BU N40-1973 / AASHTO T 275-A (abs>2%) EN 12697-6:2003
5.	G_{mbSSD} *(Saturated Surface Dry)*	$\frac{A}{B-C}$	AASHTO T 166/ ASTM D 2726 (abs<2%) EN 12697-6:2003

Legend: A = mass of the dry specimen in air; abs>2%: absorption more than 2%; B = mass of saturated-surface-dry specimen in air; B' = mass of dry and sealed specimen; C = mass of HMA sample in water; D'=mass of the dry, coated specimen; E' = mass of sealed/coated specimen under water; F =specific gravity of the coating determined at 25°C; F_p = specific gravity of the paraffin at 25°C; F_t = apparent specific gravity of plastic bag; G_{mb} = Bulk Specific Gravity; V_{DIM} = geometric volume of HMA sample; *VSD* = Vacuum Sealing Method (Corelok device).

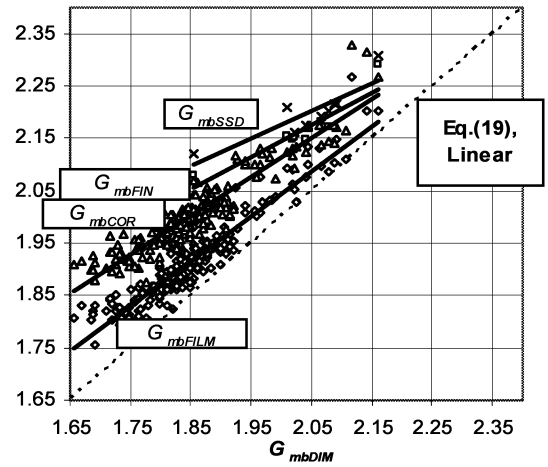

Fig. 4. G_{mbj} vs G_{mbDIM} (Linear).

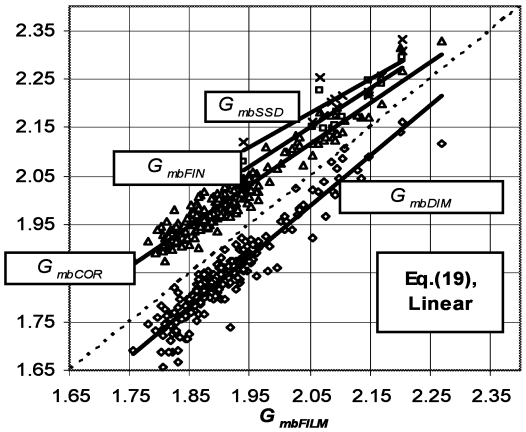

Fig. 5. G_{mbj} vs G_{mbFILM} (Linear).

specimen volume is determined as in the FILM approach but after shrink-wrapping the sample in a high-quality plastic bag, in a vacuum chamber.

Correlations

To pursue our objectives, we considered many possible relationships. Particular attention was paid to the reasons for differences among bulk specific gravity values obtained using different standards. Once the model was formalized, analysis was focused on difference dependence on mix characteristics. The following parameters were taken into account: *NMAS* = Nominal Maximum Aggregate Size; P_{200} = filler percentage (%); *S(%)* = sand percentage (%); and *b(%)* = asphalt content.

The following types of fitting curves were considered for each association of standards *i* and *j*:

$$G_{mbj} = a_{ij} G_{mbi} + b_{ij} \quad \text{(linear)} \tag{19}$$

$$G_{mbj} = G_{mbi} \pm \frac{1}{G_{mbi}^{\beta}} \quad \text{(power, asymptotic)} \tag{20}$$

$$G_{mbj} = G_{mbi} + a(G_{mm} - G_{mbi}) \quad \text{(linear, asymptotic)} \tag{21}$$

In these expressions, *j* represents the *j*-th standard used to measure G_{mbj} (*e.g.*, FILM, SSD, VSD, or FIN), whereas *i* represents the standard used to measure G_{mbi} and *a* is a coefficient.

It was necessary to split Eq. (20) into two subsets, because of different curve behaviors. Thus, curves approached to the line of equality either from above or below, depending on the standards being compared. The subset equations were:

$$G_{mbj} = G_{mbi} + \frac{1}{G_{mbi}^{\beta}}$$

(G_{mbj} approaches to G_{mbi} from above)

$$G_{mbj} = G_{mbi} - \frac{1}{G_{mbi}^{\beta}}$$

(G_{mbj} approaches to G_{mbi} from below).

In addition, the parameter β in Eq. (20) was expressed through the following equations

$$\beta^*_{ij} = b_{ij}^{I*}(\%b) + b_{ij}^{II*}(NMAS) + b_{ij}^{III*}(\%S) + b_{ij}^{IV*}(P_{200}) \tag{a}$$

$$\beta_{ij}^{**} = b_{ij}^{**}(P_{200}) \tag{b}$$

$$\beta_{ij}^{***} = b_{ij}^{***}(NMAS) \tag{c}$$

$$\beta_{ij}^{****} = b_{ij}^{****}(P_{200} + \%S) \tag{d}$$

$$\beta_{ij}^{*****} = \beta_0 + \beta_1(P_{200} + \%S) + \beta_2(NMAS) \tag{e}$$

The corresponding equations are referred to below as Eqs. (20(a)) to (20(e)).

Results

Figs. 4 to 8 and Tables 3 to 5 summarize the results. Four main classes of fitting curves were analyzed: linear (Eq. (19)), power-asymptotic (Eq. (20)), power-asymptotic with composition dependence (Eqs. (20(a)) to (20(e))), and linear asymptotic (Eq. (21)).

Eqs. (20) to (21) take into consideration the conceptual framework of Eq. (7); the predicted tendency of all G_{mb} values to reach a common asymptotic number (G_{mm}).

The data of Fig. 4 (DGFCs + PEMs) are organized as functions of G_{mbDIM}. Fig. 5 shows plots in which G_{mbFILM} is the independent variable. In Fig. 6 the independent variable is G_{mbCOR}, whereas Fig. 7 refers to G_{mbFIN} values and Fig. 8 to G_{mbSSD} data.

Fig. 4 shows the characteristics of convergence from above for all mixes and all specific gravities displayed on the y-axis. Similarly, Fig. 5 shows that when the independent variable is G_{mbFILM}, then G_{mbDIM} approaches to the line of equality from below (dotted line). Similar behavior can be seen in Figs. 6 to 8.

Table 3 contains relevant statistics and (linear) correlations. When the principal statistics are ranked for all mixes (DGFC, PEM):

$$G_{mbSSD} > G_{mbFIN} > G_{mbCOR} > G_{mbFILM} > G_{mbDIM}. \tag{22}$$

In particular, for DGFCs:

$$G_{mbDIM} = 0.97 G_{mbFILM} = 0.95 G_{mbCOR} = 0.93 G_{mbFIN} = 0.92 G_{mbSSD}.$$

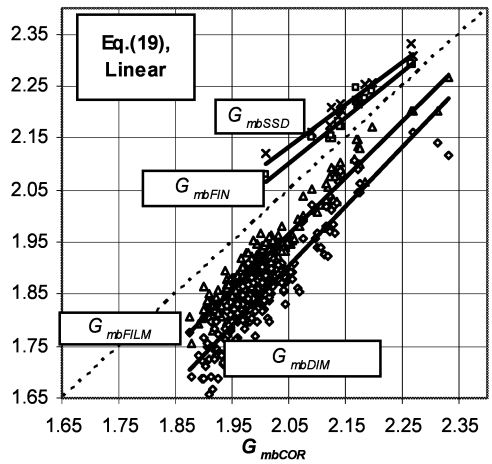

Fig. 6. G_{mbj} vs G_{mbCOR} (Linear).

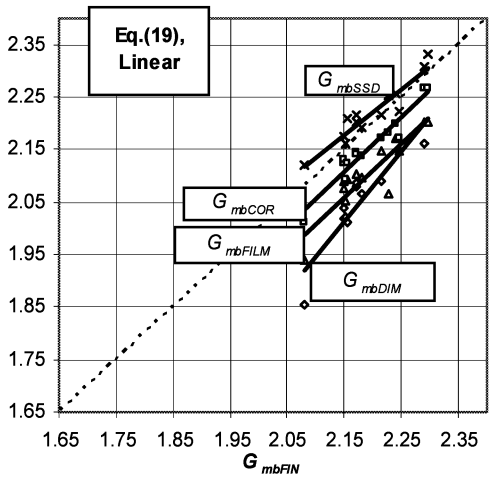

Fig. 7. G_{mbj} vs G_{mbFIN} (Linear).

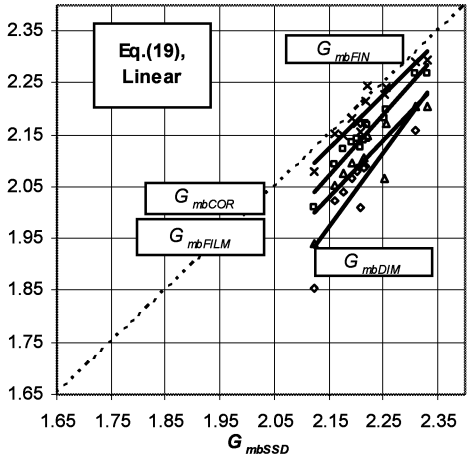

Fig. 8. G_{mbj} vs G_{mbSSD} (Linear).

Similarly, for PEMs:
$G_{mbDIM} = 0.97G_{mbFILM} = 0.92G_{mbCOR}$ and for DGFCs and PEMs:
$G_{mbDIM} = 0.96G_{mbFILM} = 0.92G_{mbCOR}$.

The skewness (S_k) values of bulk specific gravities are always positive for PEMs (more data in the right tail) and often negative for DGFCs (more data in the left tail).

It is important to observe that the dimensional method always shows the lowest skewness values.

As far as the kurtosis, k, of the probability distribution is concerned, most variance usually arises because of infrequent but extreme variations (distributions are usually leptokurtic, k>0). The coefficient of variation (CV) ranges from 2.6 to 5.0%. Note that the DIM shows the maximum value, whereas the VSD method yields low values for both DGFCs and PEMs.

In Table 3, R-square values (linear, Eq. (19)) are listed, for all five standards and three mix classes (DGFC, PEM, and DGFC + PEM).

In practice, the SSD and FIN methods were quite unreliable for

Table 3. Main Statistics and R-square Values (Two Mix Types × Five Standards).

	$\bar{x}$			σ			S_k			k			CV = (σ / $\bar{x}$) (%)		
	DGFC	PEM	DGFC + PEM	DGFC	PEM	DGFC + PEM	DGFC	PEM	DGFC + PEM	DGFC	PEM	DGFC + PEM	DGFC	PEM	DGFC + PEM
DIM	2.041	1.840	1.851	0.076	0.081	0.093	-1.280	0.706	0.838	3.720	1.67	1.112	3.7	4.4	5.0
FILM	2.100	1.906	1.920	0.069	0.075	0.090	-0.482	1.425	1.269	0.949	3.88	1.787	3.3	3.9	4.7
COR	2.153	1.995	2.007	0.064	0.068	0.080	-0.013	1.570	1.328	1.415	4.84	2.373	3.0	3.4	4.0
FIN	2.194			0.060			0.134			-0.309			2.8		
SSD	2.220			0.057			0.464			0.347			2.6		

R^2	DIM			FILM			COR			FIN	SSD
	DGFC	PEM	DGFC + PEM	DGFC	PEM	DGFC + PEM	DGFC	PEM	DGFC + PEM	DGFC	DGFC
DIM				0.861	0.859	0.891	0.864	0.819	0.851	0.818	0.739
FILM	0.861	0.859	0.891				0.833	0.890	0.916	0.817	0.757
COR	0.864	0.819	0.851	0.833	0.890	0.916				0.931	0.947
FIN	0.818			0.817			0.931				0.891
SSD	0.739			0.757			0.947			0.891	

Table 4. Main Results of Regression Analyses.

Standard Couple (y / x)	Coefficients	R^2	R^2_{ad}	Standard Couple (y / x)	Coefficients	R^2	R^2_{ad}
Linear, Eq. (19)				Power-Asymptotic, Eq. (20)			
FILM-DIM	a = 0.861; b = 0.322	0.891	0.890	FILM-DIM	β_{ij}= 4.489 (+)	0.899	0.898
COR - DIM	a = 0.741; b = 0.631	0.851	0.851	COR - DIM	β_{ij}= 3.079 (+)	0.860	0.859
FIN - DIM	a = 0.611; b = 0.923	0.818	0.795	FIN - DIM	β_{ij}= 2.875 (+)	0.833	0.812
SSD - DIM	a = 0.521; b =1.134	0.739	0.701	SSD - DIM	β_{ij}= 2.612 (+)	0.755	0.720
DIM- FILM	a = 1.034; b = -0.131	0.891	0.890	DIM- FILM	β_{ij}= 4.158 (-)	0.846	0.845
COR - FILM	a = 0.841; b = 0.392	0.916	0.916	COR - FILM	β_{ij}= 3.773 (+)	0.918	0.918
FIN - FILM	a = 0.800; b = 0.509	0.817	0.802	FIN - FILM	β_{ij}= 3.259 (+)	0.822	0.807
SSD - FILM	a = 0.700; b = 0.745	0.757	0.735	SSD - FILM	β_{ij}= 2.928 (+)	0.763	0.741
DIM - COR	a = 1.149; b = -0.450	0.851	0.851	DIM - COR	β_{ij}= 2.719 (-)	0.853	0.852
FILM - COR	a = 1.089; b = -0.226	0.916	0.916	FILM - COR	β_{ij}= 3.530 (-)	0.915	0.915
FIN - COR	a = 0.884; b = 0.291	0.931	0.925	FIN - COR	β_{ij}= 4.196 (+)	0.932	0.926
SSD - COR	a = 0.813; b = 0.468	0.947	0.942	SSD - COR	β_{ij}= 3.585 (+)	0.950	0.945
DIM - FIN	a = 1.339; b = -0.864	0.818	0.795	DIM - FIN	β_{ij}= 2.647 (-)	0.824	0.802
FILM - FIN	a = 1.021; b = -0.135	0.817	0.802	FILM - FIN	β_{ij}= 3.092 (-)	0.819	0.804
COR - FIN	a = 1.054; b = -0.158	0.931	0.925	COR - FIN	β_{ij}= 4.103 (-)	0.931	0.925
SSD - FIN	a = 0.876; b = 0.294	0.891	0.881	SSD - FIN	β_{ij}= 4.829 (+)	0.892	0.882
DIM - SSD	a = 1.417; b = -1.072	0.739	0.701	DIM - SSD	β_{ij}= 2.369 (-)	0.743	0.706
FILM - SSD	a =1.081; b = -0.293	0.757	0.735	FILM - SSD	β_{ij}= 2.738 (-)	0.760	0.738
COR - SSD	a = 1.165; b = -0.429	0.947	0.942	COR - SSD	β_{ij}= 3.453 (-)	0.948	0.943
FIN - SSD	a = 1.017; b = -0.059	0.891	0.881	FIN - SSD	β_{ij}= 4.798 (-)	0.891	0.881
Eq. (20(a))				Linear asymptotic, Eq. (21)	a = 0.08180	0.872	0.871
FILM-DIM	b^{I*}_{ij} = -0.09148; b^{II*}_{ij} = 0.21265; b^{III*}_{ij} = 0.08089; b^{VI*}_{ij} = 0.06371	0.887	0.884	FILM-DIM	a = 0.19229	0.814	0.812
COR - DIM	b^{I*}_{ij} = -0.03012; b^{II*}_{ij} = 0.14038; b^{III*}_{ij} = 0.06378; b^{VI*}_{ij} = 0.02312	0.83	0.826	COR - DIM	a = 0.28367	0.833	0.785
FIN - DIM	b^{I*}_{ij} = 0.54846; b^{II*}_{ij} = 0.15759; b^{III*}_{ij} = -0.04521; b^{VI*}_{ij} = -0.0759	0.931	0.845	FIN - DIM	a = 0.34198	0.786	0.715
SSD - DIM	b^{I*}_{ij} = 0.50692; b^{II*}_{ij} = 0.13579; b^{III*}_{ij} = -0.03267; b^{VI*}_{ij} = -0.1196	0.876	0.669	SSD - DIM	a = -0.08745	0.881	0.880
Eq. (20(b))				DIM- FILM	a = 0.12062	0.902	0.902
FILM-DIM	b^{**}_{ij} = 0.93159	0.802	0.800	COR - FILM	a = 0.22089	0.824	0.809
COR - DIM	b^{**}_{ij} = 0.60672	0.580	0.576	FIN - FILM	a = 0.28192	0.771	0.750
FIN - DIM	b^{**}_{ij} = 1.00953	0.393	0.220	SSD - FILM	a = -0.23549	0.844	0.843
SSD - DIM	b^{**}_{ij} = 0.91844	0.14		DIM - COR	a = -0.13574	0.913	0.913
Eq. (20(c))				FILM - COR	a = 0.11373	0.929	0.923
FILM-DIM	b^{***}_{ij} = 0.25679	0.840	0.838	FIN - COR	a = 0.18102	0.946	0.941
COR - DIM	b^{***}_{ij} = 0.17141	0.713	0.710	SSD - COR	a = -0.38943	0.823	0.801
FIN - DIM	b^{***}_{ij} = 0.28745	0.832	0.784	DIM - FIN	a = -0.27594	0.814	0.799
SSD - DIM	b^{***}_{ij} = 0.26103	0.755	0.673	FILM - FIN	a = -0.12562	0.927	0.921
Eq. (20(d))				COR - FIN	a = 0.07373	0.896	0.887
FILM-DIM	b^{****}_{ij} = 0.38166	0.825	0.822	SSD - FIN	a = -0.50960	0.772	0.739
COR - DIM	b^{****}_{ij} = 0.25624	0.567	0.560	DIM - SSD	a = -0.38142	0.754	0.732
FIN - DIM	b^{****}_{ij} = 0.08751	0.530	0.295	FILM - SSD	a = -0.21871	0.944	0.939
SSD - DIM	b^{****}_{ij} = 0.07966	0.484	0.174	COR - SSD	a = -0.07556	0.894	0.884
Eq. (20(e))				FIN - SSD	a = 0.08180	0.872	0.871
FILM-DIM	β_0 = 5.80379; β_1 = -0.02377; β_2 = -0.05318	0.892	0.890				
COR - DIM	β_0 = 4.65518; β_1 = -0.01742; β_2 = -0.07179	0.854	0.851				
FIN - DIM	β_0 = 0.62975; β_1 = -0.02969; β_2 = 0.32597	0.881	0.786				
SSD - DIM	β_0 = 0.62187; β_1 = -0.01454; β_2 = 0.24808	0.779	0.558				

collection of PEM data and a lower number of R-square values are therefore reported in the Table 3.

Differences between R-square values do not seem to clearly depend on mix type. As far as DGFCs are concerned, FILM, FIN, and VSD

Table 5. Differences ΔV_{j-i}

		$\Delta V_{SSD-FIN}$	$\Delta V_{FIN-COR}$	$\Delta V_{COR-FILM}$	$\Delta V_{FILM-DIM}$
DGFC	Min	-0.487	0.415	0.466	0.101
	Max	1.124	1.677	2.580	2.386
	Mean	0.460	0.858	1.168	1.017
PEM	Min			0.804	0.057
	Max			4.345	5.397
	Mean			2.377	1.913
DGFC + PEM	Min	-0.487	0.415	0.466	0.057
	Max	1.124	1.677	4.345	5.397
	Mean	0.460	0.858	2.287	1.863

data were better correlated with results from the other approaches than were SSD and dimensional data. Overall, the FILM and VSD methods were confirmed to be more closely related than were the other methods.

Table 4 summarizes the results obtained using different fitting curves. "(+)" stands for Eq. (20) used with a positive sign, and "(-)" the opposite. Note that, beside each R-square value, an adjusted R-square value is reported:

$$R^2_{ad} = 1 - \left(1 - R^2\right)\left(\frac{n-1}{n-K-1}\right) \tag{23}$$

where n is the number of observations and K is the number of independent variables.

Finally, Table 5 summarizes results derived using Eq. (18). The average values of specific volumes are positive, although some negative values were obtained when comparing SSD and FIN.

The following observations may be made:

1. Eqs. (19) to (21) yield, in general, similar R-square values.
2. In particular, the power-asymptotic law yields the best R-square values (R^2_{ad}= 0.71-0.95, $\beta \approx$ 2.4-4.8). These values are generally higher than those obtained using the linear-asymptotic curve (Eq. (21)) or the linear expression (Eq. (19)).
3. When the coefficient β in the power-asymptotic equation is expressed as a function of mix characteristics (Eqs. (20(a)) to (20(e))), no appreciable optimization is obtained. Interesting results are seen when NMAS is analyzed (R^2_{ad}= 0.67-0,84, Eq. (20(c)).
4. In linear regression, the highest R-square value is always referable to a relationship between the SSD and VSD methods (R^2_{ad}= 0.94, DGFCs), whereas the lowest R-square value is seen when SSD and Dimensional (DGFCs) are compared. The VSD, FILM, and FIN methods are well-correlated with all remaining methods. In particular, the method explains, on average, 91% of VSD variance, 87% that of FIN, 85% that of FILM, 84% that of SSD, and 83% that of DIM.
5. The linear equation (Eq. (19)) shows quite good performance but this does not necessarily consider any tendency toward the equality line.
6. The power-asymptotic equations (Eq. (20)) show very good "performance" (in terms of R^2_{ad}) but there is a small drawback in that a few standards showed changes in functional signs. It is very interesting to observe that transportability seems to be quite immediate and coefficients are contained within a small range (2.4-4.8). Note that this range becomes even smaller when SSD and DIM models are not considered (the range is then 3.1-4.3).
7. The power-asymptotic equations in which composition parameters are included (Eqs. (20(a) to (20(e)) seem not to offer significant optimization from either a conceptual viewpoint or when quantitative-fitting was analyzed.
8. The linear-asymptotic curves (Eq. (21)) are both significant and interesting. Moreover, these curves do not have the drawback of a sign change (all a values have proper signs). They confirm the conceptual framework outlined above, but G_{mm} calculation appears to be more a conceptual than a practical necessity.
9. Another question to be considered deals with the robustness and logical admissibility of the three classes of fitting curves. In fact, both linear curves (Eq. (19)) and linear asymptotic curves (Eq. (21)) are associated with the possibility that two different fitting curves G_{mbj} and G_{mbk}, both expressed as functions of a third (G_{mbi}), may intersect on the graph (for example, Figs. 4, 7, and 8). This means that the relationship between any two methods j and k changes (from > to < or *vice versa*), perhaps because of statistical defects. On the contrary, when $\beta_1 \neq \beta_2$, there is no possibility that two curves of the power–asymptotic type (Eq. (20)) can intersect.
10. Regarding the four differences ΔV_{j-i} (Eq. (18)), Table 5 shows that the lowest difference usually relates to the SSD-FIN comparison, whereas the highest difference is seen in the comparison of COR and FILM.

Further, although the averages are always positive (and agree with Eqs. (15) and (22)), significant deviations can be easily detected when SSD and FIN methods are compared.

Concluding Remarks

Transportability of bulk specific gravities is a theoretical and practical necessity and, in this paper, constituted our main objective.

The following conclusions were reached:

1. Even if there is a need for further research, the formalized model, in which the higher the specific gravity the lower the differences between different measurement methods, appears to be basically validated.
2. The discretization of volumes used in the model offers a simple and intuitive tool for interpreting differences among methods.
3. The introduction of composition parameters (such as NMAS) does not yield any significant improvement in the regressions.
4. Parafilm, vacuum-sealing, and paraffin procedures (even if not applicable to PEMs) emerge as possible key methods.
5. The vacuum-sealing method is the best descriptor of the other methods.
6. Linear relationship evaluation is efficient but power-asymptotic curves are more robust and preferable from a theoretical viewpoint. In particular, power-asymptotic curves yield a well-grounded logical algorithm permitting an approach to the issue of G_{mb} transportability.

References

1. Brown, E.R., Hainin, M.R., Cooley, A., and Hurley, G., (2004). Relationship of Air Voids, Lift Thickness, and Permeability in Hot Mix Asphalt Pavements, *NCHRP Report 531*, *National Center for Asphalt Technology, Auburn University, Auburn, AL*, Transportation Research Board, Washington, D.C., USA.
2. Cooley, L.A. Jr., Prowell, B.D., Hainin, M.R., Buchanan, M.S., and Harrington, J., (2002). Bulk Specific Gravity Round-Robin Using the Corelok Vacuum Sealing Device, *Report 02-11, FHWA-IF-02-044*, National Center for Asphalt Technology, Auburn, AL, USA.
3. Crouch, L.K., Badoe, D.A., Cates, M., Borden, T.A., Copeland, A.R., Walker, C.T., Dunn, T., Maxwell, R.A., and Goodwin, W.A., (2003). Bulk Specific Gravity of Compacted Bituminous Mixtures: Finding a More Widely Applicable Method, *Final Report, Project Number TNSPR-RES1153*, Department of Transportation, Tennessee, USA.
4. Kvasnak, A., Williams, C.R., Williams, B., and Stanton, B., (2006). Evaluation of Methods Used to Determine Bulk Specific Gravity of Hot Mix Asphalt, *10th International Conference on Asphalt Pavements*, Quebec City, Quebec, Canada, CD-ROM.
5. Mohammad, L.N., Herath, A., Wu, Z., and Cooper, S.A., (2005). Comparative Study of Factors Influencing the Permeability of Hot-Mix Asphalt Mixtures, T*he Journal of the Association of Asphalt Paving Technologists*, Vol. 74E, AAPT Publications, CD-ROM.
6. Montepara, A. and Virgili, A., (1996). La Determinazione Della Massa Volumica e dei Vuoti nei Cnglomerati Bituminosi Aperti, *Proceedings of the SIIV Conference*, Società Italiana Infrastrutture Viarie, Ancona, Italy, pp. V163-V170.
7. Spellerberg, P. and Savage D., (2004). An Investigation of the Cause of Variation in HMA Bulk Specific Gravity Test Results Using Non-Absorptive Aggregates, *Project 9-26 (Phase 2)*, *Web Document 66*, National Cooperative Highway Research Program, http://onlinepubs.trb.org/Onlinepubs/nchrp/nchrp_w66.pdf.
8. Williams, R.C., Williams, B., Stanton, B., KvasnaK, A., and Van Dam, T., (2005). Development of Acceptance Criteria of Compacted Hot Mixture Asphalt Bulk Specific Gravity Based on Vacuum Sealed Specimens, *Final Report No. RC-1522,* Construction and Technology Division, Michigan Department of Transportation, Lansing, MI, USA.